ARTICLE   OPEN

Hurricane stalling along the North American coast and implications for rainfall

Timothy M. Hall [ID][1] and James P. Kossin[2]

The average speed of tropical cyclone (TC) translation has slowed since the mid 20th century. Here we report that North Atlantic (NA) TCs have become increasingly likely to "stall" near the coast, spending many hours in confined regions. The stalling is driven not only by slower translation, but also by an increase in abrupt changes of direction. We compute residence-time distributions for TCs in confined coastal regions, and find that the tails of these distributions have increased significantly. We also show that TCs stalling over a region result in more rain on the region. Together, increased stalling and increased rain during stalls imply increased coastal rainfall from TCs, other factors equal. Although the data are sparse, we do in fact find a significant positive trend in coastal annual-mean rainfall 1948–2017 from TCs that stall, and we verify that this is due to increased stalling frequency. We make no attribution to anthropogenic climate forcing for the stalling or rainfall; the trends could be due to low frequency natural variability. Regardless of the cause, the significant increases in TC stalling frequency and high potential for associated increases in rainfall have very likely exacerbated TC hazards for coastal populations.

INTRODUCTION

A TC's trajectory largely determines its hazard. The most obvious example is whether or not a TC makes landfall and, if so, where. Another factor affecting hazard is the length of time a TC resides in a region near the coast; i.e., whether the TC "stalls" near the coast. A stalling TC inflicts strong winds on the same region for a longer time, potentially driving greater storm surge and depositing more rain.

Recent analysis of observations indicates that the average translation speed of TCs has slowed globally since the mid 20th century, including overland regions of the North Atlantic (NA) domain.[1] TC trajectories are largely determined by the steering of large-scale mid-tropospheric circulation patterns and a generally smaller beta effect due to gradients in planetary vorticity that induces a poleward drift.[2] Research is conflicted concerning the evolution of the atmospheric circulation in response to anthropogenic climate forcing. Some modeling and observational analyses suggest a weakening of general atmospheric circulation patterns, including those of the tropics.[3–6] In one study, simulated TCs using climate-model-projected circulation changes indicate reduced westward steering flow in the NA subtropics and a consequential reduction in westward moving tracks compared to recurving tracks,[7] though elsewhere in the NA the projected changes in the magnitude of steering flow are negligible. Another recent study found that the translation speed of NA TCs is reduced under climate-change scenarios.[8] By contrast, other work, including high-resolution doubled-CO_2 modeling experiments[9] and downscaled CMIP3 and CMIP5 late-21st-century modeling experiments,[10] find no significant change in TC track speed.

In the mid-latitudes, some results suggest that a reduction in meridional temperature gradients due to arctic amplification has reduced the speed and increased the waviness of mid-tropospheric zonal winds[11–13] in winter as well as summer.[14] These weaker and more variable winds provide less robust steering flow for TCs and allow blocking patterns to persist longer. However, there is considerable debate on the robustness of the signal and the physical mechanisms.[15,16]

Taken together, there is not at present a clear mechanism explaining the observed TC speed reduction. Nonetheless, the observation of slower TC translation[1] has the potential for elevating hazard, and it is worthwhile exploring its impacts. One key impact is that slower TCs are more prone to stalling, and stalling TCs have the potential for depositing damaging amounts of rain. This trajectory-induced increase in rainfall is exacerbated by the climate-warming impact on the hydrologic cycle. Increased atmospheric moisture enhances the likelihood of extreme rainfall events of all types.[17,18] Close to the center of a TC, the increases in rain rate can reach 10% per degree C of warming in some model projections,[19] exceeding the 7% dictated by the Clausius-Clapeyron relationship. There is evidence that TC rainfall has increased over the southeastern US in recent decades, both absolutely and as a fraction of extreme rainfall on the Continental United States (CONUS).[20] Hurricane Harvey's catastrophic flooding of 2017 was a tragic example of a stalled TC over extremely warm ocean water that produced record rainfall.[21] According to recent studies, a significant fraction (9–37%) of Harvey's rainfall was due to a warming climate,[22,23] and the frequency of Harvey-like rainfall events is projected to increase substantially by the late 21st century.[24]

Here we define a stalling metric for TCs and report that the stalling frequency of NA TCs has increased significantly in coastal regions since the mid 20th century. We then show that accumulated TC rainfall increases with increased TC residence over a coastal region. Together, the observations that the frequency of stalls has increased and that stalling TCs accumulate more rain imply an increase in rainfall from TCs, other factors

[1]NASA Goddard Institute for Space Studies, New York, NY, USA and [2]NOAA National Centers for Environmental Information, Center for Weather and Climate, Madison, WI, USA
Correspondence: Timothy M. Hall (timothy.m.hall@nasa.gov)

equal. We find a positive trend from 1948–2017 in annual rainfall from stalling TCs on CONUS, and we show that increased stalling frequency drives the trend.

To examine the stalling behavior of NA TCs and its impact on rainfall, we use observational records to compute annual time series of TC translation speed, directional variability, stall frequency, and rainfall. For TC track characteristics, we use the National Hurricane Center HURDAT2 data[25] from 1944 to 2017. HURDAT2 track points labeled as extra-tropical are excluded, in order to focus on TCs only. The start date of 1944 roughly corresponds to the era of routine aircraft reconnaissance. Our primary focus is coastal regions, due to the hazard. In addition, pre-satellite era HURDAT2 data are more reliable near the coast;[26] nearly all landfalling TCs are likely to have been monitored in some form after about 1900.[27] For rainfall we use the CPC 0.25° daily gridded CONUS precipitation data from 1948–2017, a dataset derived from the CONUS rain-gauge network.[28]

RESULTS

Translation speed and directional deviations

For TC translation speed, we compute the annual-mean 6-hourly rate of translation, that is, the distance the TC center translates in 6 h divided by 6 h, averaged over all the 6-hourly TC increments in a year. We restrict attention to HURDAT2 track points within 200 km from the North-American coast (both water and land sides), defined by 50 km coastal segments spanning Yucatan to Maine. In addition, we exclude HURDAT2 track points indicated as extra-tropical in order to focus on TCs. Over the 1944-2017 period, the annual mean coastal NA TC speed has fallen from 18.6 to 15.5 km h^{-1}, about 17% (Fig. 1a). This speed reduction is consistent with previous results,[1] which showed a translation speed reduction over North American land. We also compute the annual values of the 0.05 quantile; i.e., the 6-hourly speed that is slower than all but 5% of the 6-hourly speeds in a year. The

reduction in speed of these very slow coastal track segments is more pronounced: the 0.05 quantile has decreased from 7.7 to 4.8 km h^{-1}, about 38% (Fig. 1b). According to bootstrap tests and Student's t-tests, the negativity of these trends is significant (see Methods).

In addition to the translation speed, we find an increasing tendency for abrupt changes in NA TC track direction. Such changes can be measured by a "displacement angle," the angle between one 6-h track increment and the next. (The dot products between successive 6-h vectors are computed and converted to angles.) In the coastal NA, the annual-mean displacement angle has increased by about 27%, from 17.8° to 22.6°. Meanwhile, the annual 0.95 quantile (the angle that is greater than 95% of displacement angles in a year) has increased by about 32%, from 43.6° to 57.7°. The positivity of the mean-angle trend is significant by bootstrap and Student's t-tests. The significance of the positivity of the 0.95-quantile angle trend is marginal; 96.2% of bootstrap resamples have a positive trend, but the Student's t-test does not quite reject the non-positive-trend null hypothesis ($p = 0.061$, see Methods).

To check sensitivity to changes in observations before and during the satellite era, we also compute trends starting from the years 1970–1979 (Fig. 1, blue). Trends in the mean translation speed and mean and quantile angular deviations from the 1970s–2017 all exhibit the same sign as 1944–2017. The exception is the quantile translation speed, for which 1970s–2017 trend magnitudes are reduced, and 3 of 10 of the 1970s–2017 trends switch sign. As for the stall-fraction time series (Fig. 3b), the 1970s–2017 trends (not shown) are in fact more positive than the 1944–2017 trend.

All of the 1970s–2017 trends in Fig. 1 have significance levels below 95%. However, by itself this does not impugn the significance of 1944–2017 trends. A characteristic of subsets of a time series with a trend plus noise is that the subset trends are less significant. To demonstrate this, for each variable, we construct 1000 1944–2017 synthetic time series, specified to have the
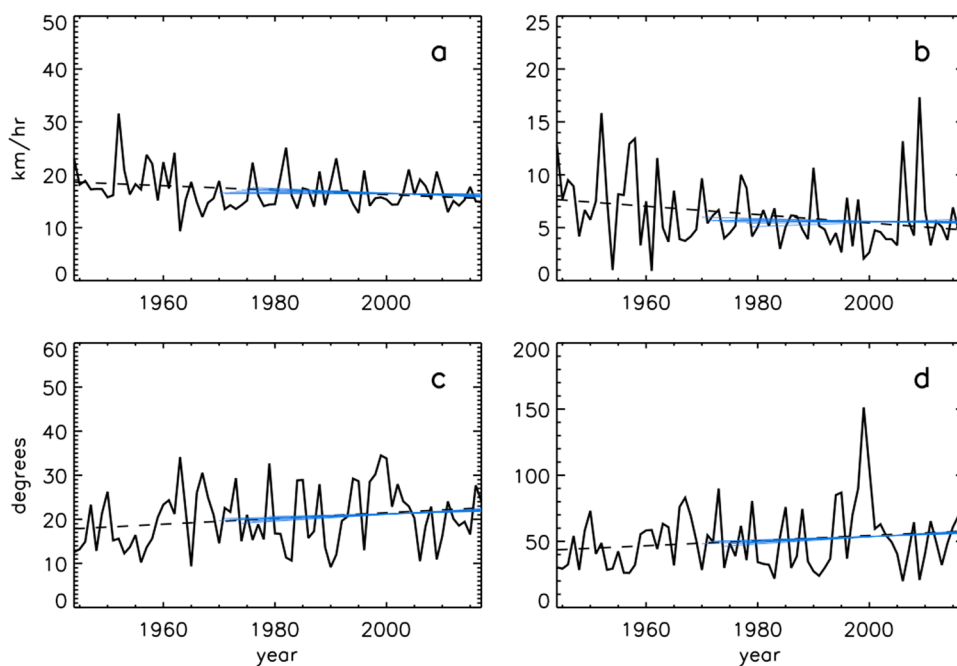

Fig. 1 Time variation of tropical cyclone track speed and angular deviation. **a** The annual-mean North Atlantic TC translation speed for track steps within 200 km from the North-American coast from 1944–2017. **b** The 6-hourly speed at the 0.05 quantile. **c** The annual-mean angle between successive 6-hourly coastal TC track vectors from 1944–2017. **d** The angle between successive 6-hourly TC track vectors at the 0.95 quantile. In each panel, a trend line is shown (dashed). The signs of the trends are significant according to bootstrap tests. According to Student's t-tests the signs of trends are also significant, expect for the 0.95-quantile angle, which is marginally insignificant (see Methods). Also shown (blue) are trend lines computed starting from each of the years 1970–1979, representing the start of the era of satellite observation
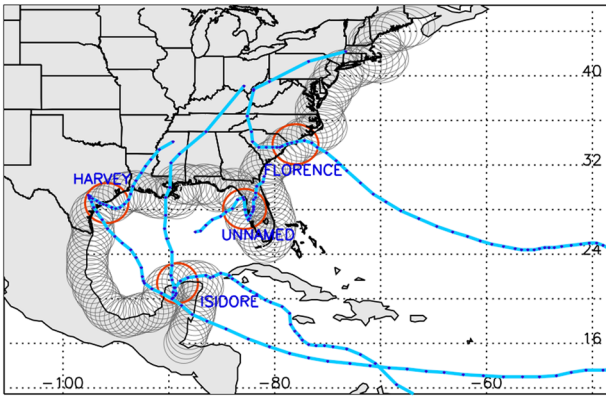
Fig. 2 Examples of four TCs (blue) that stalled near the coast: Unnamed (1968), Isidore (2002), Harvey (2017), and Florence (2018). Also shown are the 200-km coastal impact regions lining the coast in which residence-time distributions and stalls are computed. In the impact regions shown in red the illustrative TCs resided for at least 48 h. Longitude and latitude are labeled at bottom and right

observed 1944–2017 trend, but differing due to randomization of the annual residuals about the trend. For each synthetic time series we compute trends on the 1970s–2017 subsets. The 5–95% spread on each of the 1970s–2017 trends across the 1000 samples indicates the uncertainty expected when computing trends on a subset of a longer time series with a significant trend plus noise. For all four variables, the 5–95% synthetic trend intervals span the observed 1970s–2017 trends. It is possible that observational sampling changes affect the time series, but their impacts cannot be distinguished from the 1944–2018 trend plus noise. We conclude that 1970s–2017 trends are consistent with 1944–2017 trends.

Coastal stalling frequency

Reduced speed and increased directional deviations both play a role in increasing the probability that a track "stalls" near the coast, spending many hours over a confined region. Reduced speed has the obvious effect of increasing the time over a region, while directional deviations elevate the chance of meandering within the region before exiting. Examples of four NA TC tracks exhibiting stalls near the North American coast are shown in Fig. 2.

In order to quantify changes in the frequency of stalling, we construct a distribution of impact-region track residence times. An impact region is defined as the region encompassed by a circle of radius R about a fixed point of interest $\mathbf{x}$. The time, τ, that a track resides inside the region is recorded. Most tracks don't cross through a specified impact region, and $\tau = 0$ for those tracks; for the few tracks that do cross through the region, $\tau > 0$. We form a distribution of residence times, $F(\tau, \mathbf{x})$, over the tracks in a season and average over the points $\mathbf{x}$ in a domain of interest to obtain $F(\tau)$. We are interested in the behavior of tracks that actually pass through impact regions, so we only use values at $\tau \geq 1$ h for the distribution. We normalize each year's averaged distribution, to remove the impact of varying seasonal TC number. The resulting diagnostic—an annual impact-region residence-time distribution—represents the distribution of time spent residing in an impact region in a given year, among the tracks that cross into the region, averaged over all the impact regions in the domain.

To examine trends in stalling in North-American coastal regions of the NA, we average 162 impact regions of 200-km radius centered on coastal mileposts spaced at 50 km spanning Yucatan to Maine (Fig. 2). In this domain, of the 1110 HURDAT2 TCs 1944–2017, there are 130 TCs and 831 total instances in which a track spends $\tau > 36$ h in a coastal impact region. (A single track can reside for 36 + hours in several overlapping or disjoint regions.) Of

these 831 instances, 452 experience a 6-hr direction deviation of at least 45°. Using a more stringent residence-time threshold of 48 h, there are 66 TCs and 358 total instances, of which 235 have direction deviations of at least 45°. Note that as the residence-time threshold is increased, a greater fraction of the instances displays large directional deviations. Longer stalls are more likely to incorporate meanders.

Figure 3a shows residence-time distributions averaged over the coastal impact regions. The distributions are accumulated over 1944–1980 (blue) and 1981–2017 (red), the first and second halves of the period. Both distributions peak around $\tau = 10$ h; if a track enters within R of $\mathbf{x}$, it's more likely to spend at least a few hours, than just barely graze the circle for 1 h.

It is the behavior of the tail of $F(\tau)$, however, that is of most interest to us, because it represents the frequency of stalling TCs. Residing more than 48 h inside a 200 km region can be taken as a reasonable definition of a TC "stall," and the 1981–2017 tail crosses above the 1944–1980 for τ between 36 and 48 h. We integrate the annual distributions above 48 h to form the time series shown in Fig. 3c. These values represent the annual fraction of the TCs that pass through a 200 km impact region that spend at least 48 h inside the region, averaged over the coastal regions.

There is considerable variability in the annual coastal stalling fraction of Fig. 3c, in part due to poor sampling. To contribute to the stalling fraction, a TC has to both pass into a coastal impact region and spend 48 + hours within the region. Although all 74 years have had TCs that enter coastal impact regions, only 66 TCs have resided 48 + hours in a region, for a total of 358 stalling events accumulated over the regions. For many of the years, no stalls occur. Nonetheless, the distribution of stalling TCs across the 74-year period shown in Fig. 3e indicates an increase in frequency. For example, 30 of the 66 stalling TCs occur in the last-third of the period (1993–2017), while only 17 occur in the first-third (1944–1968). Assuming a random distribution of 66 events in 74 years, the probability that the final 25 years has at least 13 more events than the first 25 years is only 0.03.

Bootstrap tests, Student's t-tests, first-half/second-half tests, and generalized jackknife tests in which the coastal impact regions are randomly subsampled, all confirm the significance of the stalling fraction shown in Fig. 3c (see Methods). We have also tested the sensitivity to the possibility of underreporting in sparsely populated regions in the early part of the record. We compute the stalling-fraction time series restricted to just US coastal regions (light blue, Fig. 3b), representing a 109-region subset of the full 162 coastal impact regions. The result is very similar and also displays a significant positive trend. We conclude that NA TCs are stalling near the coast with increasing frequency.

The 200 km radius of the impact zones represents a subjective balance between resolving geographic structure and including sufficient events. To examine sensitivity to the impact region size, we also perform the analysis using smaller coastal impact regions, $R = 150$ km. The distributions (not shown) decline more rapidly with τ. It's more difficult for a TC to reside for long periods in a smaller region, and there are fewer TCs (32) that reside 48 + hours in a region. The inter-annual time variation in the distribution tail, however, is qualitatively similar to the $R = 200$ km case, showing a positive trend for the frequency of 48 + hour stalls. For $R = 100$ km, however, there are only 8 TCs that spend 48 +hours inside the regions, too few to calculate trends.

We have focused on trends in TC stalls in coastal regions, because TCs pose the greatest hazard to coastal regions, and because the HURDAT2 track data from the pre-satellite era are more reliable near the coast.[27] However, we have also performed a basin-wide NA analysis. We define 200 km impact regions centered on the 2511 points of a 1° grid from 100°W-20°W and 10° N-40°N, a domain spanning the TC-active NA. The results for the residence-time distributions, the 48 + hour stalling time series, and annual stalling TC count time series (Fig. 3b, d, f) are similar to
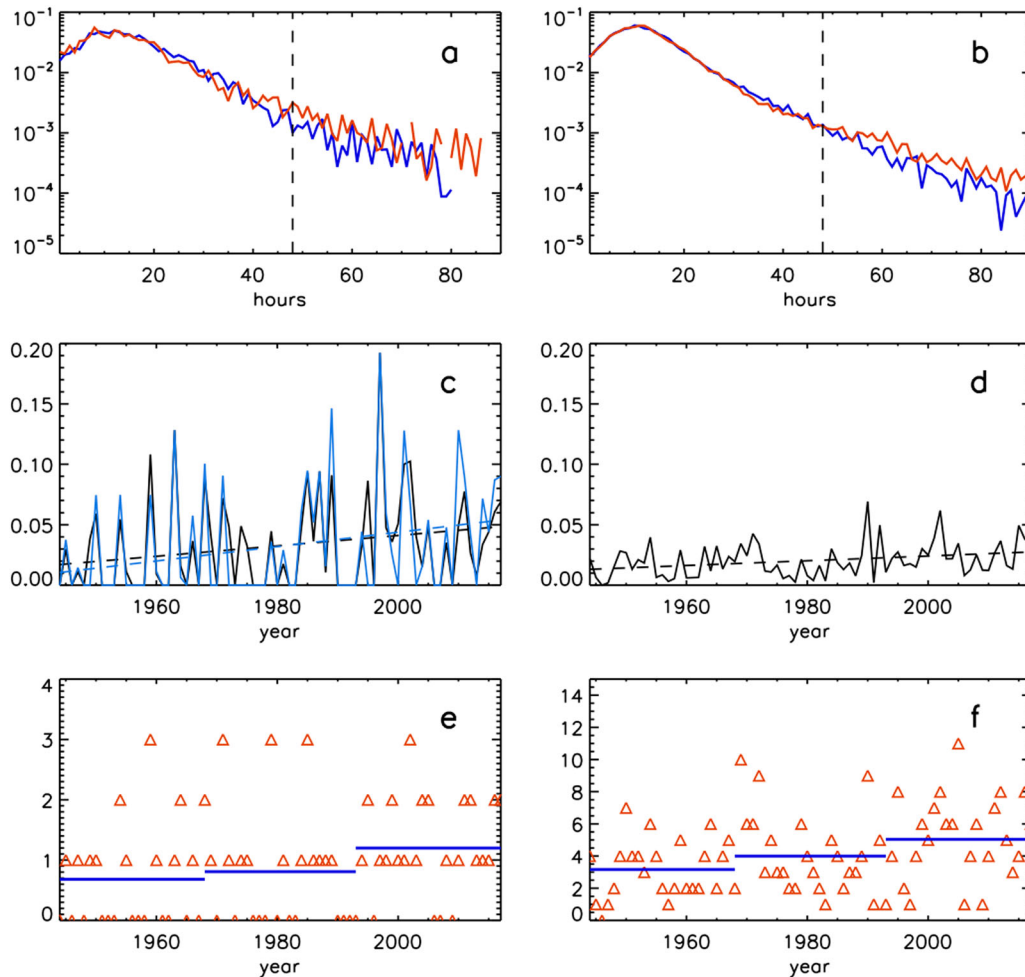
Fig. 3 Analysis of tropical cyclone stalling. **a** Distributions of residence time, averaged over the 200 km coastal impact regions shown in Fig. 2. Blue is accumulated over 1944–1980 and red over 1981–2017, the first-half and second-half of the 1944–2017 period. The vertical dashed lines indicates the 48-h residence-time threshold. **b** As in panel a, but averaged over 200 km impact regions that span the TC-active North Atlantic, 100°W-20°W and 10°N-40°N. **c** The time series of the annual coastal distributions integrated above 48 h (black). This represents the annual fraction of the TCs that pass through a 200 km coastal impact region that reside at least 48 h inside the region, averaged over the coastal regions. Also shown (light blue) is the same time series, but restricted to impact regions along the US coast. **d** As in panel **c**, but for the basin-wide North Atlantic distributions illustrated in panel **b**. In panels **c** and **d** linear trends are indicated as dashed lines, and they are significantly positive (see Methods). **e** Annual count of TCs that reside at least 48 h in a coastal impact region (symbols) and the annual-mean counts over the time periods 1944–1968, 1968–1993, and 1993–2017, roughly equal thirds of the 1944–2017 period (blue). **f** As in panel (**e**), but for TCs that reside at least 48 h in one of the impact region spanning the TC-active North Atlantic

the coastal analysis. On a basin-wide scale, as well as near the coast, TCs are stalling with increasing frequency, though there is less confidence in data quality.

Reduced translation speed and increased meandering both play a role in increased TC stalling. To examine further the relationship among stalling, translation speed, and meandering, we compute the annual fraction of coastal 48 + hour stalls that exhibit an angular deviation of 60° or more (Fig. 4). The time series is noisy; not all years have 48 +hour stalls, and many have only a few, so that the fraction with large deviations is poorly sampled. The second half of the 1944–2017 period (from 1981) has a higher fraction (0.61) than the first half (0.44). Bootstrap tests indicate that the positivity of this first-second half difference is marginally significant; 95.1% of re-samples have a fraction greater in the second half period than first. It is possible that increasingly long stalls offer increasingly more opportunity for large angular deviations. It is also possible that the increased fraction is a reporting artifact, resulting from less accurate TC location estimates in the earlier data record (see Discussion).

Rainfall analysis

Greater accumulated rainfall is one of the primary hazards of TCs stalling over coastal regions. If a TC resides longer in a region, then, on average, it is natural to expect that the TC deposits more rain on the region. To verify this, we compute the accumulated rain per TC within 100 km of TC centers on the overland-part of HURDAT2 tracks in the CONUS coastal impact regions (Fig. 2). Typical radial rainfall distributions peak around 50 km from TC centers,[29] so that 100 km should capture the bulk of TC-related rainfall. Figure 5 shows the accumulated rainfall per TC as a function of TC residence time in the regions. There is a clear increase in accumulated rain per TC with residence time. Figure 5 also shows the accumulated rain per TC in the impact regions partitioned by stalling ($\tau \geq 48$ h) and non-stalling ($\tau < 48$ h) TCs and during the first-half (1948–1982) and second-half (1983–2017) of the CPC data period. Stalling TCs rain more in both the first and second-half of the period than non-stalling TCs. On the other hand, there is little variation in rain per TC between the time periods for either stalling or non-stalling TCs.

The observations that, 1, accumulated rainfall increases with residence time and, 2, TCs are stalling more over coastal regions imply an increase in annual rainfall from stalling TCs. To check this, for each TC that stalls ($\tau > 48$) inside a coastal impact region of Fig. 2, we accumulate the rainfall over the CONUS CPC 0.25° grid cells that lie within 100 km of the TC center. We average the values annually and compute the linear trend in time (Fig. 6a, red curve). From 1948 to 2017 this annual-mean coastal rainfall from stalling TCs has a positive trend of 0.026 km^3 yr^{-1}, and the positivity is significant at the 96.5% level by bootstrap tests (see Methods). This trend corresponds to a factor 3.2 increase in annual-mean rain
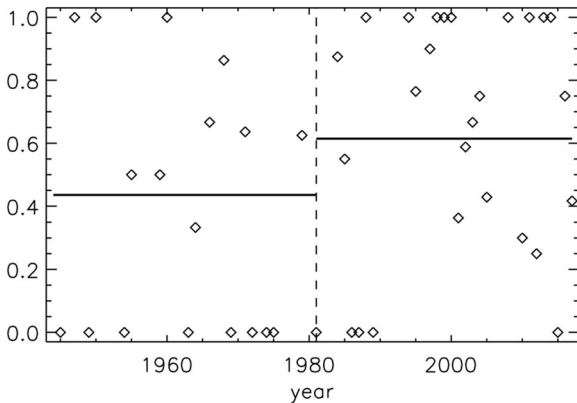
from stalling TCs from 1948 to 2017, roughly consistent with the factor 2.6 increase in TC coastal stalling frequency (Fig. 3b).

Comparing the first-half and second-half of the data period, we find that annual-mean rain for stalling TCs has more than doubled from 0.97 km^3 yr^{-1} for 1948–1982 to 2.01 km^3 yr^{-1} for 1983-2017. This increase could be due to increased rain per stalling TC or increased frequency of stalling TCs. To distinguish between these possibilities we compute the mean rain per stalling TC, which is 2.65 km^3 for the first half and 2.56 km^3/stall for the second half, essentially unchanged, as shown in Fig. 5. By contrast, the annual-mean stalling fraction per coastal impact region (Fig. 3b) is 0.024 yr^{-1} for the first half and 0.038 yr^{-1} for the second half, a 58% increase. We conclude that increased stalling is causing the increased annual-mean coastal rain from stalling TCs.

The stalling-TC rain signal is noisy; several factors contribute to annual variability in rainfall, and there are only 50 stalling-TC landfalls on CONUS over the 1948–2017 period. To test sensitivity of the stalling-TC rain trend to individual events, we remove the single largest event (Tropical Storm Allison, 2001) and find that the trend drops from 0.026 to 0.020 km^3 yr^{-1}. When the second, third, and fourth largest events, Georges (1998), Fay (2008), and Harvey (2017), are removed one at a time the trend drops to 0.022, 0.018, and 0.015 km^3 yr^{-1}, respectively. When all of these top four events are removed, the positive trend vanishes. Overall, bootstrap tests indicate that 96.3% of resamples have a positive sign, but clearly sampling is poor, and there is high sensitivity to the few largest events. However, the probability that the top 4 out of 50 events randomly occur in the most recent 20 of 70 years is only 0.007. Thus, a null hypothesis that these intense rain events are randomly distributed over the 1948–2017 period is violated, corroborating the straightforward expectation that increased TC stalling frequency enhances annual-mean rain from stalling TCs.

Annual-mean rain from all TCs is a combination of the rain from stalling and non-stalling TCs (Fig. 6b). In contrast to stalling TCs,

Fig. 4 Angular deviation stalling fraction. Annual fraction of 48 + hour stalls in coastal impact regions (Fig. 2) that exhibit angular deviations of 60° or more (symbols). Values are only plotted for years that have at least one such stall. Horizontal line segments indicate the mean fractions before and after 1981 (dashed line), the first half and second half of the period
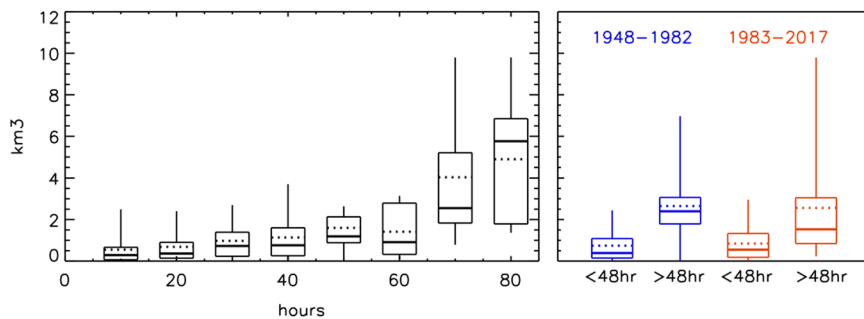

Fig. 5 TC rain variation with residence time. (left) Accumulated rain per TC within 100 km of TC centers while TCs are in the CONUS coastal impact regions of Fig. 2 as a function of residence time in the regions. Box and whisker plots show the medians (solid), means (dotted), 25–75% quantiles (box), and 2.5–97.5% quantiles (whiskers) over all TCs and regions at each 10-hr residence time bin. (right) Box and whisker plots of the same accumulated rain per TC, now separately in the periods 1948–1992 (blue) and 1983–2017 (red) that have residence times less than and greater or equal to 48 h, as labeled
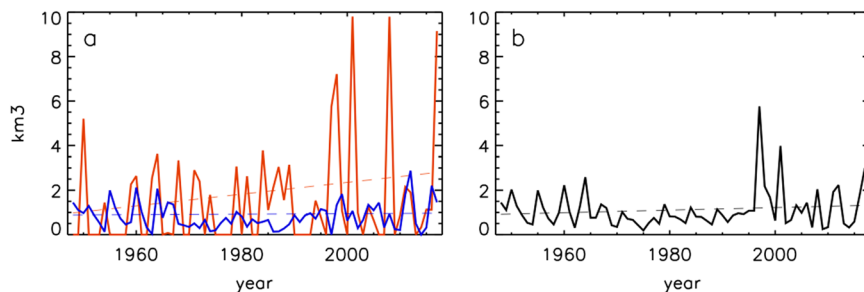

Fig. 6 Annual TC rain. **a** Annual-mean accumulated CONUS TC rainfall within 100 km of the TC center while TCs are in coastal impact regions. Red indicates stalling TCs; i.e., TCs that reside at least 48 h in an impact region. Blue indicates TCs that do not stall. Dashed lines indicate linear trends. **b** The total annual-mean rain per TC from both stalling and non-stalling TCs (solid) and its linear trend (dashed)

annual-mean rain from non-stalling TCs has not increased significantly (Fig. 6a, blue curve). The combined effects of an increase in annual rainfall from stalling TCs and no increase from non-stalling TCs is a weaker overall increase: from 1948 to 2017 annual-mean coastal rainfall from all TCs has increased by about 40% with a linear trend of 0.0059 km^3 yr^{-1}. However, the positivity is not significant; only 91% of bootstrap re-samples have a positive trend, and the Student's t-test does not reject the non-positive-trend null hypothesis ($p = 0.14$). Knight and Davis[20] also found evidence of increases in TC rainfall extremes, as well as increases in the fraction of CONUS rainfall extremes due to TCs. These researchers attribute the increase to TC intensity and frequency, but as their focus was extreme one-day rain events, they would not have picked up stall-driven rain signals accumulated over several days.

In addition to sampling uncertainty, there are uncertainties driven by features of the CPC dataset, such as changes in rain-gauge density and technology through time[30] and the errors associated with gauge-based rain collection at high wind speeds.[31] It is also possible that weak coherent low-frequency variability in the TC-rainfall time series (see below) may compromise the bootstrap tests somewhat, which assume statistical independence of the regression residuals. Thus, 96% for stalling TCs and 91% for all TCs are upper bounds on the significance of the respective annual-mean TCs rainfall trend.

DISCUSSION

We have found evidence for an increase in the frequency of NA TCs stalling over coastal regions, as well as throughout the NA basin. It is important to note, however, that the HURDAT2 data on which the analysis is based are not homogenized for trend analysis.[26,27,32,33] They are "best track" data; that is, they are based on the best observational sources available at the time. Since these observational sources have changed over time, sampling artifacts can be an issue in trend analysis. This is less so for TC position, which is easier to observe than intensity.[26] Still, it is worth examining possible biases.

It is possible that TC locations have been reported with increasing precision over time. For example, observations to fix the location of TC centers were enhanced in the 1970s, the dawn of the satellite era. In the earlier portion of our 1944-2017 record, a poorly-known 6-hourly position might have been assigned an interpolated value between better-known positions,[34,35] a report-ing practice that would have become less common as monitoring improved. Such a reporting bias would underestimate translation speed in the early years, because it would result in smoother tracks (less gross distance traveled) over the same amount of time, thus creating an artificial speed increase through time. Such an increase is in contrast to the decrease we report. Thus, to the extent such a bias exists, its correction would only further enhance the reduction in translation speed.

An early-record bias toward smoother tracks could indeed cause an artificial positive trend in track directional deviations. However, it wouldn't cause an artificial trend in stalling frequency. It would merely shift the stalls from straight-line speed-reduction to speed-reduction plus meandering, a hint of which is seen in Fig. 4. In addition, the fact that the positive stalling trend is seen in coastal regions, as well as over the full NA, supports the validity of the result. In the pre-satellite era, TCs were better observed near the coast than over open ocean,[26,27] and their positions were more accurately known. However, we see a positive trend in stalling frequency in coastal regions, as well as over the full NA.

We make no attribution to anthropogenic forcing of the trends in TC stalling frequency and associated annual-mean coastal TC rainfall, and the trends reported here could be due to low-frequency natural variability. Many factors influence TC rainfall, including sea-surface temperature (SST). In the time series of Fig. 6

the reduction below the trend line from roughly 1970 to 1990 and the elevated values before and after are reminiscent of the Atlantic Multidecadal Oscillation (AMO),[36] a mode of climate variability defined by multi-decadal variations in NA SST. In fact, annual-mean non-stalling TC rain is 64% higher when the AMO is above average than below, a difference that is significant at >99% level by bootstrap tests. (For this analysis, the AMO has been detrended over 1948–2017.) The AMO-associated difference in annual-mean stalling TC rain, however, is a smaller 34%, and is not significant. The annual stalling-frequency (Fig. 3b) also displays no significant AMO relationship according to this test.

Our work has revealed a significant increase since the mid 20th century in the stalling frequency of TCs near the North-American coast. We have also found that annual-mean rainfall from stalling TCs on the U.S. has risen significantly due to the increased stalling frequency. The increased stalling is due to both a reduction in TC translation speed and a trend toward large and abrupt deviations in direction. Even as the original version of this article was being prepared for submission, Hurricane Florence was stalling over coastal North Carolina and dropping record amounts of rain on the region. Our analysis on the National Hurricane Center's preliminary Public Advisory reporting of Florence's track indicates that the hurricane's center spent 53 h in the 200km-radius coastal impact region centered on 78.0°W and 33.9°N (Bald Head Island, North Carolina), qualifying as a stall. Hurricane Harvey in 2017, and now Hurricane Florence in 2018, are archetypical of the hazard that stalling hurricanes pose for coastal populations. A positive trend in stall frequency and the possibility of increased rain may need to be taken into account in planning for future TC flood risk.

METHODS

Translation speed and angular deviations were computed from the HURDAT2 1944-2017 archive downloaded from https://www.nhc.noaa.gov/data/hurdat/hurdat2-1851-2017-050118.txt. The translation speed was computed as the distance between successive 6-hourly storm center latitude-longitude positions divided by 6 h. The angular deviation between two successive 6-hourly track vectors v_1 and v_2 is $\theta = \cos^{-1}(v_1 \cdot v_2/|v_1||v_2|)$. Daily accumulated 0.25° gridded CONUS rainfall data were downloaded from https://www.esrl.noaa.gov/psd/data. The daily accumulated values were divided by four when summing over regions surrounding 6-hourly HURDAT2 locations. The rest of our methodology addresses issues related to the trend analysis of time series, as described below.

Significance of trend signs

To test the significance of the sign of time-series trends we use a block-bootstrap approach,[37,38] as well as one-tailed Student's t-test. In block-bootstrap tests, time series are first segmented into a series of N adjacent time windows or blocks, choosing the blocks such that regression residuals whose times are centered at adjacent blocks are uncorrelated. Then, multiple N-block series are randomly re-sampled with replacement from the original series. A re-sampled series consists of N randomly selected blocks, with the ith block consisting of the time-series value, Y_i, associated with the block's center. Note that some blocks may be selected multiple times, and others not at all. For example, in the case of annual blocks, a re-sampled time series might have three copies of the pair (1965, Y_{1965}) and none of (2013, Y_{2013}). In this way, the sequence in time of the of the original series is maintained, but various re-sampled values in the series will randomly receive more or less (or no) weight.

We check for serial correlation of the regression residuals by computing lag-one autocorrelation coefficients (ACCs). For lag-one auto-correlated processes, correlations decrease exponentially with time, and the timescale to de-correlate is $T_{DC} = -\Delta t/\ln(C)$, where Δt is the time step, here one year, and C is the ACC. Within time intervals T_{DC}, residuals are correlated, but at greater temporal separations they are approximately uncorrelated. For all of the time series discussed here $T_{DC} < 1$ year, so that bootstrap re-sampling of annual values is appropriate. For each series being tested we generate 100,000 annual-bootstrap re-samples, and compute the trend for each re-sample. We then count the fraction of the re-samples whose trend
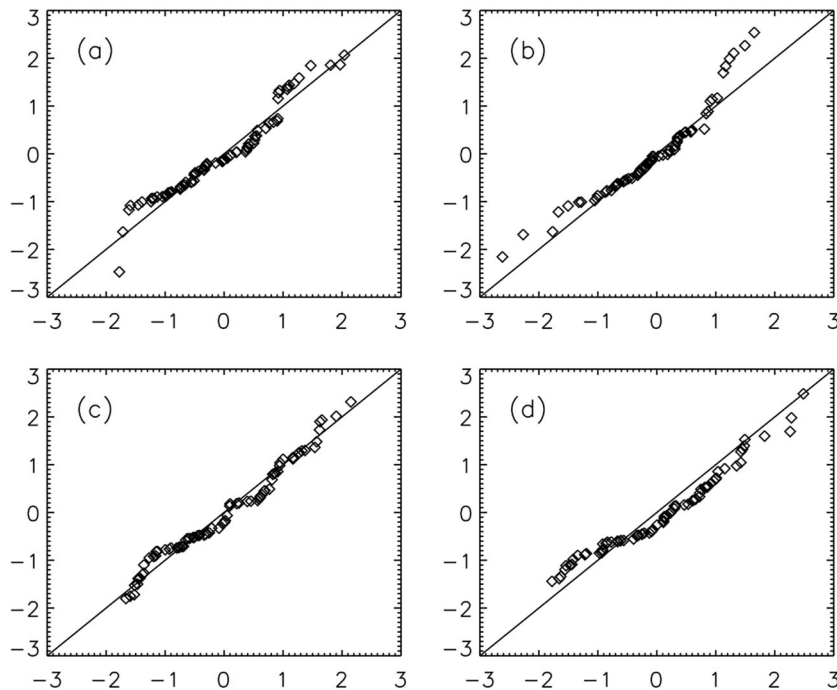
Fig. 7 QQ plots of speed and angular deviation. QQ plots of regression residuals of (**a**) mean translation speed, (**b**) 0.05 quantile translation speed, (**c**) mean angular deviation, (**d**) 0.05 quantile angular deviation. Residuals are plotted on the y axes and standard normal deviates on the x axes

is the same sign as the trend in the original time series. We call the trend's sign significant if at least 95% of the re-sample trends have the same sign.

For Student's t-tests the same criterion of uncorrelated residuals applies. The degrees of freedom used for the t-tests is N_{eff}-2, where N_{eff} is the number of independent time-series blocks. We use one-tailed testing because we are testing whether the observed sign of a positive (negative) trend is significantly greater (less than) than zero. For example, for a positive observed trend the null hypothesis of non-positive trend is violated for our significance criterion if the t statistic corresponds to a probability $p < 0.05$, in which case we say the trend is significantly positive.

Translation speeds and angular deviations

For the annual mean translation speed (Fig. 1a), from the bootstrap tests, of the 100,000 re-samples, 99.2% of the trends are negative. For annual 0.05 quantile track speed (Fig. 1b) 97.3% of the trends are negative. For the annual mean angular deviation (Fig. 1c), of the 100,000 re-samples, 97.9% of the trends are positive. For annual 0.95 quantile angular deviation (Fig. 1c), 96.2% of the trends are positive. Using the Student's t-tests, the trend in mean translation speed is significantly negative ($p = 0.014$), the trend in 0.05 quantile track speed is significantly negative ($p = 0.013$), and the trend in mean angular deviation is significantly positive ($p = 0.037$). By the t-test, however, the positive trend in 0.95 quantile angular deviation is marginally insignificant ($p = 0.061$). We have also computed quantile-quantile (QQ) plots for the translation speed and angular deviation residuals (Fig. 7). No large deviations from normality are indicated.

Stalling frequency

For the $R = 200$ km coastal stalling frequency time series (Fig. 3b), of the 100,000 bootstrap re-samples, 99.0% of the trends are positive. For the $R = 200$ km basin-wide stalling frequency time series (Fig. 3d), 99.8% of the bootstrap trends are positive. By the Student's t-test the coastal and basin-wide stalling time series are also both significantly positive ($p = 0.02$ and $p = 0.005$ respectively). The QQ plot of the residuals, however, shows large deviations from normality (Fig. 8). This is not surprising, as the annual stall fraction is restricted to lie between zero and one, and hence the distribution cannot be normal.

As an alternative test of the sign of the stall frequency trend, we compare the first half of the period (1944–1980) to the second half
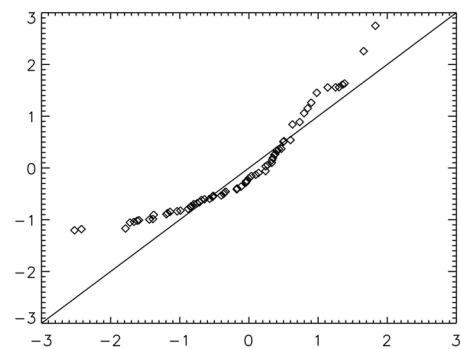

Fig. 8 QQ plot of regression residuals of the coastal stalling frequency (Fig. 3b). Residuals are plotted on y axes and standard normal deviates on x axes

(1981–2017). Across 100,000 bootstrap re-samples of the complete 1944–2017 stall-frequency time series, we compute the means of these first-half and second-half 37-year periods. In 98.6% of the re-samples, the 1981–2017 mean is greater than the 1944–1980 mean.

To further test the significance of the time series trend, we perform a generalized jackknife test on the coastal impact regions. First, we select every 8th 200-km impact region to form a subset of regions that do not overlap. (The full set of 200 km-radius regions have centers that are spaced at 50 km along the coast; the new set of 200 km-radius regions have centers that are spaced at 400 km making them approximately non-overlapping.) Then, among this 20-region non-overlapping set, we construct 1000 subsets, each consisting of 16 randomly-selected distinct regions (80% of the complete non-overlapping set), and compute the 48 + hour stalling trends on each. We find that 97.4% of the 1000 subsets display positive trends.

Annual TC-track CONUS rainfall time series

For the stalling-TC rainfall time series of Fig. 6a, 96.5% of the 100,000 annual time-series re-samples have positive slopes. The Student's t-test

also shows significant positivity ($p = 0.027$). We also compare the average annual-mean stalling-TC rain between the first-half (1948–1982) and second-half (1983–2017) periods: across the 100,000 bootstrap resamples, 97.8% have a higher value in the second-half period. As a further test, in addition to performing the bootstrap analysis by re-sampling among the annual-mean stalling-TC rainfall values, we have also re-sampled among the individual stalling TC rain values and constructed the annual-mean rainfall time series from these resamples. The results are very similar: 95.9% of the 100,000 time series formed in this way exhibit a positive trend. Sensitivity tests to removing individual high-rain TCs are described in the main text. For the full TC rain series (stalling plus non-stalling) of Fig. 6b, only 91% of 100,000 re-samples have a positive sign, and the Student's t-test does not reject the non-positive-trend null hypothesis ($p = 0.14$).

DATA AVAILABILITY

Tropical cyclone data are provided by the Hurricane Research Division of NOAA's AOML and are available at www.aoml.noaa.gov/hrd/hurdat/hurdat2.html. CPC US Unified Precipitation data are provided by the NOAA/OAR/ESRL PSL, Boulder, CO, from their website www.esrl.noaa.gov/psd/. All figures are based on these data. The AMO monthly time series, used for analysis discussed in the text, is freely available from climatedataguide.ucar.edu/climate-data/atlantic-multi-decadal-oscillation-amo.

CODE AVAILABILITY

Code used to analyze these data are available upon request to the authors.

AUTHOR CONTRIBUTIONS

Authors T.M.H. and J.P.K. both performed analysis on TC stalls, comparing and contrasting different metrics, before settling on the version shown here. The final analysis on TC stalling described here and shown in the figures was performed by T.M.H. T.M.H. and J.P.K. first performed independent analysis on the rainfall data, comparing calculations to confirm that the same results were achieved. The final rainfall figures shown here were generated by T.M.H. T.M.H. also performed the bootstrap significance testing of the time series, and these results were confirmed by J.P.K. using alternative methods. T.M.H. and J.P.K. are equally responsible for interpretation of the results. T.M.H. performed the majority of initial manuscript preparation and modifications in response to reviewer comments, with additional input and editing provided by J.P.K.

ADDITIONAL INFORMATION

Competing interests: The authors declare no competing interests.

Publisher's note: Springer Nature remains neutral with regard to jurisdictional claims in published maps and institutional affiliations.

REFERENCES

1. Kossin, J. P. A global slowdown of tropical-cyclone translation speed. *Nature* **558**, 104–107 (2018).
2. Holland, G. J. Tropical cyclone motion: environmental interaction plus a beta effect. *J. Atmos. Sci.* **40**, 328–342 (1983).
3. He, J. & Soden, B. J. Anthropogenic weakening of the tropical circulation: the relative roles of direct CO_2 forcing and sea surface temperature change. *J. Clim.* **28**, 8728–8742 (2015).
4. Vecchi, G. A. & Soden, B. Global warming and the weakening of the tropical circulation. *J. Clim.* **20**, 4316–4340 (2007).
5. He, C., Wu, B., Zou, L. & Zhou, T. Responses of the summertime subtropical anticyclones to global warming. *J. Clim.* **30**, 6465–6479 (2017).
6. Mann, M. E. et al. Influence of anthropogenic climate change on planetary wave resonance and extreme weather events. *Sci. Rep.* **7**, 19831 (2017).
7. Colbert, A. J., Soden, B. J., Vecchi, G. A. & Kirtman, B. P. The impact of anthropogenic climate change on North Atlantic tropical cyclone tracks. *J. Clim.* **26**, 4088–4095 (2013).
8. Gutmann, E. D., Rasmussen, R. M., Changhai, L. & Ikeda, K. Changes in hurricanes from a 13-Yr convection-permitting pseudo–global warming simulation. *J. Clim.* **31**, 3643–3657 (2018).
9. Kim, H.-S. et al. Tropical cyclone simulation and response to CO_2 doubling in the GFDL CM2.5 high-resolution coupled climate model. *J. Clim.* **27**, 8034–8054 (2014).
10. Knutson, T. R. et al. Dynamical downscaling projections of twenty-first century Atlantic hurricane activity: CMIP3 and CMIP5 model-based scenarios. *J. Clim.* **26**, 6591–6617 (2013).
11. Coumou, D., Lehmann, J. & Beckmann, J. The weakening summer circulation in the northern hemisphere mid-latitudes. *Science* **348**, 324–327 (2015).
12. Francis, J. A. & Vavrus, S. J. Evidence linking Artic amplification to extreme weather in mid-latitudes. *Geophys. Res. Lett.* **39**, L06801 (2012).
13. Vavrus, S. J. et al. Changes in North American circulation and extreme weather: Influence of Artic amplification and Northern Hemisphere snow cover. *J. Clim.* **30**, 4317–4333 (2017).
14. Coumou, D., Di Capua, G., Vavrus, S., Wang, L. & Wang, S. The influence of Arctic amplification on mid-latitude summer circulation. *Nat. Comm.* **9**, 2959 (2018).
15. Barnes, E. A. Revisiting the evidence linking Artic amplification to extreme weather in midlatitudes. *Geophys. Res. Lett.* **40**, 1–6 (2013).
16. Cohen, J. et al. Recent Artic amplification and extreme mid-latitude weather. *Nat. Geosci.* **7**, 627–637 (2014).
17. Hartmann, D. L. et al. In *Climate Change 2013: The Physical Science Basis*. (eds. Stocker, T. F. et al.) Contribution of Working Group I to the Fifth Assessment Report of the Intergovernmental Panel on Climate Change 159–254 (Cambridge University Press, Cambridge, 2013).
18. Prein, A. F. et al. Increased rainfall volume from future convective storms in the US. *Nat. Clim. Change* **7**, 880–884 (2017).
19. Knutson, T. R. Global projections of intense tropical cyclone activity for the late 21st century from dynamical downscaling of CMIP5/RCP4.5 scenarios. *J. Clim.* **28**, 7203–7224 (2015).
20. Knight, D. B. & Davis, R. E. Contribution of tropical cyclones to extreme rainfall events in the southeastern United States. *J. Geophys. Res.* **114**, D23102 (2009).
21. Trenberth, K. E., Cheng, L., Jacobs. P., Zhang, Y. & Fasullo, J. Hurricane Harvey links to ocean heat content and climate change adaptation. *Earth Future*. https://doi.org/10.1029/2018EF000825 (2018).
22. Van Oldenborgh, G. J. et al. Attribution of extreme rainfall from Hurricane Harvey. *Env. Res. Lett.* **12**, 124009 (2017).
23. Wang, S.-Y. S. et al. Quantitative attribution of climate effects on Hurricane Harvey's extreme rainfall in Texas. *Env. Res. Lett.* **13**, 054014 (2018).
24. Emanuel, K. Assessing the present and future probability of Hurricane Harvey's rainfall. *Proc. Nat. Acad. Sci.* **114**, 12681–12684 (2017).
25. Landsea, C. W. & Franklin, J. L. Atlantic hurricane database uncertainty and presentation of a new database format. *Mon. Wea. Rev.* **141**, 3576–3592 (2013).
26. Landsea, C. W. Counting Atlantic tropical cyclones back to 1900. *EOS Trans., Am. Geophys. Union* **88**, 197–208 (2007).
27. Landsea, C. W. et al. Impact of duration thresholds on Atlantic tropical cyclone counts. *J. Clim.* **23**, 2508–2519 (2010).
28. Chen, M., Xie, P., Janowiak, J. E. & Arkin, P. A. Global land precipitation: A 50-year monthly analysis based on gauge observations. *J. Hydrometeorol.* **3**, 249–266 (2002).
29. Lonfat., M., Marks, F. D. & Chen, S. S. Precipitation distribution in tropical cyclones using the Tropical Rainfall Measuring Mission (TRMM) microwave imager: a global perspective. *Mon. Wea. Rev.* **132**, 1645–1660 (2004).
30. Chen, M. et al. Assessing objective techniques for gauge-based analysis of global daily precipitation. *J. Geophys. Res.* **113**, D04110 (2008).
31. Medlin, J. M., Kimball, S. K. & Blackwell, K. G. Radar and rain gauge analysis of the extreme rainfall during Hurricane Danny's (1997) landfall. *Mon. Weather Rev.* **135**, 1869–1888 (2007).
32. Vecchi, G. A. & Knutson, T. R. Estimating annual numbers of Atlantic hurricanes missing from the HURDAT database (1878–1965) using ship track density. *J. Clim.* **24**, 1736–1746 (2011).
33. Landsea, C. W. et al. A reanalysis of the 1911-20 Atlantic hurricane database. *J. Clim.* **21**, 2138–2168 (2008).
34. Delgado, S., Landsea, C. W. & Willoughby, H. Reanalysis of the 1954-63 Atlantic hurricane seasons. *J. Clim.* **31**, 4177–4192 (2018).
35. Hagen, A. B., Strahan-Sakoskie, D. & Luckett, C. A reanalysis of the 1944-53 Atlantic Hurricane seasons—The first decade of aircraft reconnaissance. *J. Clim.* **25**, 4441–4460 (2012).
36. Schlesinger, M. E. & Ramankutty, N. An oscillation in the global climate system of period 65-70 years. *Nature* **367**, 723–726 (1994).
37. Efron, B. & Tibshirani, R. J. *An Introduction to the Bootstrap*. (Chapman and Hall, New York, 1993).
38. Vogel, R. M. & Shallcross, A. M. The moving blocks bootstrap versus parametric time series models. *Wat. Res. Res.* **32**, 1975–1882 (1996).